Combinatorial catalyst approach for high-density growth of horizontally aligned single-walled carbon nanotubes on sapphire

Ago, Hiroki
Institute for Materials Chemistry and Engineering, Kyushu University

Nakamura, Yumiko
Institute for Materials Chemistry and Engineering, Kyushu University

Ogawa, Yui
Graduate School of Integrated Frontier Sciences, Kyushu University

Tsuji, Masaharu
Institute for Materials Chemistry and Engineering, Kyushu University

出版情報：Carbon. 49 (1), pp.176-186, 2011-01. Elsevier
バージョン：

Combinatorial catalyst approach for high-density growth of horizontally aligned single-walled carbon nanotubes on sapphire

Hiroki Ago,*[,a] Yumiko Nakamura,[a] Yui Ogawa,[b] and Masaharu Tsuji,[a]

[a] *Institute for Materials Chemistry and Engineering, Kyushu University, Kasuga, Fukuoka 816-8580, Japan*

[b] *Graduate School of Integrated Frontier Sciences, Kyushu University, Fukuoka 816-8580, Japan*

We studied effects of metal catalyst and gas composition on the chemical vapor deposition (CVD) growth of horizontally aligned single-walled carbon nanotubes (SWCNTs) on r-plane sapphire substrates. The SWCNTs are sitting on the substrate and aligned along [$1\bar{1}01$] direction of the sapphire surface. A combinatorial metal deposition method was applied for single and binary metal catalysts to systematically investigate the thickness and the composition dependence. The horizontally-aligned SWCNTs grown from stripe-patterned catalysts enable the direct comparison of the catalytic activity based on nanotube density. We found that the SWCNT density strongly depends on the metal catalyst in the order Fe>Co>>Ni≈Cu, while no nanotubes were grown over Mo. In addition, the methane concentration during CVD strongly influenced the nanotube density, and the optimal concentration varied depending on the metal species and its thickness. The study on the binary metal catalysts revealed that Fe-Co combination increases the SWCNT density (7~9 tubes/μm) about twice of the original metal film. The Co-Cu binary catalyst also showed the high density (8~10 tubes/μm) under a limited methane concentration. Different catalytic activity of each metal is discussed.

---

* Corresponding author: Fax: +81-92-583-7817, E-mail: ago@cm.kyushu-u.ac.jp (H. Ago)

1. Introduction

Single-walled carbon nanotubes (SWCNTs) with one-dimensional hollow structure composed of sp^2 carbon network have attracted a great interest from their excellent electrical, mechanical, and thermal properties [1]. It has been demonstrated that SWCNTs show high carrier mobility (~3,000 cm^2/Vs [2]) and high current density (10^9 A/cm^2 [3]). The mobility is higher than that of Si devices (electron and hole mobilities are 1500 and 450 cm^2/Vs, respectively) [4]. SWCNTs show unique electronic structure which varies from metallic to semiconducting depending on the chirality and diameter. Their transport properties can be applied to electronics for various purposes: semiconducting tubes are expected for field-effect transistor (FET) and sensor applications, while metallic tubes are suitable for transparent electrodes [5-8].

When SWCNTs are grown on a plain SiO_2/Si wafer, nanotubes grow in random direction, forming random network of SWCNTs [9]. The random network is also prepared by wet processes, such as ink-jet printing and drop-casting of the SWCNT dispersion [7,10]. These random networks can average out the transport properties of metallic and semiconducting tubes, thus making device operation more reproducible [10-13]. Recent development of metal-semiconductor separation techniques realized the fabrication of the devices enriched with semiconducting or metallic SWCNTs [5-8]. However, the transport properties of the random network, such as current and operation frequency, are limited by the inevitable inter-tube hopping, because charge carriers injected from an electrode need to migrate multiple nanotubes to reach another electrode.

For the improvement of device performance as well as integration of a number of SWCNTs for more advanced electronics, horizontal alignment of SWCNTs (i.e. SWCNTs are parallel with each other sitting on the substrate) is of great importance. Direct growth of horizontally aligned SWCNTs has been achieved by using electric field or laminar gas flow during the chemical vapor deposition (CVD) growth [14-17]. Also, the surface-guided growth has been proposed on single-crystal substrates [18-27] and trenched SiO_2/Si wafers [28-30]. Among these, the lattice-oriented mechanism observed on the single-crystal substrates, such as sapphire (α-Al_2O_3) [19-22] and quartz (α-SiO_2) [23-27], has attracted a

great interest because the substrates can give high-density SWCNT array with high degree of alignment. The alignment is explained by the anisotropic van der Waals interaction between SWCNTs and the crystalline surface, which originated in the anisotropic surface atomic arrangement (in other words, surface atomic rows) of the single crystal planes [19,31]. The synthesis of highly aligned SWCNT arrays is advantageous for device fabrication [32,33]. However, for many applications, higher density is demanded for better device performance. For example, high frequency application requires a dense SWCNT array because the large tube spacing increases the parasitic capacitance [34]. The high nanotube density is also important for high current operation of transistors and for low resistivity of nanotube-based transparent electrodes.

On single-crystal quartz, a high SWCNT density of 8-10 tubes/μm has been reported from several groups [25,35-37]. It is demonstrated that the CVD with ethanol source can give higher density, as high as 22 tubes/μm [38]. We note that all these works have used single metal catalyst and no binary metal catalysts have been studied. On the other hand, on sapphire, the reported average SWCNT density (0.5-5 tubes/μm [19-22]) is generally lower than that on quartz. However, we observed interesting growth modes of SWCNTs, such as unidirectional growth [39] and orthogonal growth [40] which are attributed to the unique anisotropic surface arrangement of sapphire. The direct growth of bent SWCNT growth was also demonstrated by making artificial steps perpendicular to the alignment direction [41]. Moreover, it is proposed that chiral angle of aligned SWCNTs depends on crystal planes of sapphire [42], which suggests the strong influence of atomic arrangement of sapphire surface not only on the growth direction but also on the nanotube chirality. Therefore, it is important to investigate the high density growth of SWCNTs on sapphire substrates.

In the CVD growth of SWCNTs, it is widely known that some binary metal catalysts improve the nanotube yield. Vertically aligned SWCNTs were first synthesized over the Co-Mo binary metals using ethanol as carbon source [43]. Systematic study of the vertically aligned tubes over the Co-Mo catalyst was demonstrated by using a combinatorial mask deposition (CMD) method [44]. This method offers deposition of single or binary metal films with different thickness on one substrate and helps to evaluate the catalytic activity in

terms of the film thickness and/or chemical compositions. It is suggested that Mo stabilizes the catalytically active metal nanoparticles by forming $CoMoO_x$ layer at the interface between the substrate and the metal nanoparticle [44]. The Co-Mo combination has also been applied to grow SWCNTs with a narrow chirality distribution using carbon monoxide as carbon source [45]. Interestingly, the optimal metal catalyst strongly depends on gas source [9]. For methane source, Fe-Mo combination gives high growth yield [46,47]. Therefore, applying binary metal catalysts to the growth of horizontally-aligned SWCNTs is interesting, because they can potentially increase the nanotube density. An advantage of the horizontally-aligned array is that we can directly count the SWCNT density by scanning electron microscope (SEM) observation to assess the catalytic activities of various metal catalysts.

Here, we investigate the activity of single and binary metal catalysts by applying a CMD approach to obtain a high density SWCNT array. The SWCNT density was found to greatly depend on metal catalyst and methane concentration. Specific combinations of binary metals, Fe-Co and Co-Cu, showed a dramatic increase in the SWCNT density.

2. Experimental

2.1. Catalyst preparation

Sapphire r-plane substrates with negligible miscut (<0.3º) were purchased from Kyocera Co., Japan. As-received substrates were cut into 10 mm×10 mm, cleaned by sonicating in acetone, and then spin-coated with photoresist. A stripe pattern, 10 μm opening with 300 μm spacing, was created by ultraviolet exposure and development. We modified the CMD method proposed by Noda et al. [44] by using a stripe-patterned substrate which is specifically designed for the horizontally-aligned nanotube growth (Fig. 1). The substrate with patterned photoresist was placed 5 mm below the mask with a 2 mm-width slit for the deposition of metal film with a gradual film thickness. The distance from the center of the slit to the origin of the stripe pattern was set at 3 mm. Five transition metals, Fe, Co, Ni, Cu, and Mo, were studied as catalysts. A metal film was deposited on the substrate through the slit by a radio-frequency (RF) magnetron sputtering (Shibaura Mechatronics Co., CFS-4ES)

in Ar atmosphere at 0.6 Pa with a power of 200-300 W. For the study of binary metal catalyst, the mask was rotated by 90º after the deposition of the first metal. Finally, the resist was removed with acetone, followed by cleaning with O_2 plasma treatment under 100 W for 0.5 sec.

2.2. Carbon nanotube growth

A substrate with patterned catalyst was placed in a quartz tube with 26 mm inner diameter and heated in Ar flow (300 sccm). After reaching 900 ºC, Ar gas was switched to H_2 gas (100 sccm) to reduce the metal catalyst and clean the sapphire surface. After 5 min, a controlled amount of CH_4 gas was introduced with H_2 gas with a total flow rate of 380 sccm for 15 min. Then, the sample was cooled down to room temperature in the Ar flow.

2.3. Characterization

Samples were characterized with a SEM (HITACHI S-4800) equipped with a stage controller, an atomic force microscope (AFM, Veeco Nanoscope IIIa), and a Raman microscope (JASCO, NRS-2100). The nanotube density was measured by SEM at the fixed catalyst lines and positions by moving the sample with the stage controller.

3. Results and discussion

3.1. Single metal catalysts

Figure 1a,b shows the schematic of the preparation method of catalyst lines by combining the CMD method with photolithography patterning. Through a 2 mm-width slit, metal vapor was deposited on the sapphire substrate. Here, the thickness of the deposited metal film has the maximum at just below the slit and decreases gradually with increasing distance from the slit. For the estimation of the film thickness at each patterned line, we deposited a relatively thick metal film and measured the height of the metal films after lift-off. , Deposition rate was determined from the height profile measured by AFM, and it was used to estimate the nominal thickness of each line of stripe pattern. Shown in Fig. 1c is the nominal thicknesses

of metal catalysts calculated from the corresponding deposition rates. The decay curves of nominal thicknesses can be fitted with exponential curves [44].

CVD was performed over the patterned substrates with a mixed flow of CH_4 and H_2 at 900 ºC. The growth temperature was set 900 ºC, because we observed the highest SWCNT density for the Fe catalyst at this temperature. During the CVD process, the patterned metal film is converted to metal nanoparticles that act as the catalyst for the nanotube growth. On sapphire r-plane, as-grown SWCNTs are horizontally aligned as illustrated in Fig. 1d. In our experiments, the methane concentration, defined as $[CH_4]/([CH_4]+[H_2])\times100$ (%), was changed from 30-90% while keeping the same total flow rate, because we found that the methane concentration influences the nanotube yield much stronger than the CVD temperature does.

Figure 2 shows SEM images of horizontally aligned nanotubes grown from the patterned Fe, Co, Ni, and Cu metals. As confirmed by Raman spectroscopy, the white lines correspond to SWCNTs which looks thicker due to the charging effect [31]. No nanotube growth was seen for the Mo metal. The SWCNT density varied with the metal thickness (i.e. the distance from the slit) and the supplied methane concentration. The SEM images shown in Fig. 2 present the highest density areas obtained with the optimized thickness and methane concentration. We found that Fe and Co metal catalysts give high SWCNT density. The maximum nanotube density is 4~6 tubes/μm for both Fe and Co catalysts, which is determined by counting the number of tubes in 1 μm width. On the other hand, Ni and Cu metals gave low SWCNT density (~1 tube/μm) even with the optimized metal thickness and methane concentration.

The high degree of alignment is seen for all the catalysts that grow SWCNTs. This represents that the alignment is originated in SWCNT-sapphire interaction [31], because the metal species does not influence the nanotube alignment. The high degree of alignment can be explained by the well-ordered dense atomic rows of the sapphire surface (spacing <2 nm); even if a SWCNT escapes from the one atomic row, it will be soon caught by neighboring rows thus making the tube straight. We note that it is not straightforward to estimate the SWCNT yield for the powder catalysts [46,47]. This is because the weight gain of the

catalyst measured after the CVD used to determine the SWCNT yield cannot exclude the possible contribution of amorphous carbon formation. On the other hand, the horizontally-aligned tubes give more reliable estimation of the catalytic activity by directly counting the SWCNTs.

We studied the influence of CH_4 concentration on the SWCNT growth. Figure 3 compares the SWCNT density observed for five different metals. We found that Fe catalyst showed the highest SWCNT density under a wide reaction window; the nanotube growth was observed in the 35-85% CH_4 concentrations. In general, too high CH_4 concentration deactivates the metal nanoparticle catalyst, because the particles tend to be covered with amorphous carbon. On the other hand, under too low CH_4 concentration, the carbon supply is not enough to nucleate and grow a nanotube. Therefore, the high catalytic activity observed for the Fe metal under wide CH_4 concentrations is outstanding. This indicates strong catalytic activity of the Fe metal toward SWCNT growth for, at least, CH_4 source.

Co metal also showed the high SWCNT density comparable to Fe metal (Fig. 3). However, Co showed much narrower growth window than the Fe metal in terms of the CH_4 concentration. In addition, the peak maxima observed for the Co metal shifts to lower CH_4 concentration compared with the Fe metal. These results suggest that Co is more easily deactivated by excess carbon. Mizuno et al. reported selective combination of metal catalyst and carbon source; Fe metal prefers hydrocarbon feedstock (ethylene) to grow SWCNTs, while Co metal prefers alcohol (ethyl alcohol) feedstock [9]. We speculate that Co metal can show high catalytic activity with alcohol, because the oxygen-containing species formed by the alcohol decomposition can etch excess amorphous carbon formed over the Co nanoparticles, leading to the extended catalyst lifetime. The Co metal also showed weak catalytic activity under lower CH_4 concentrations (<50%). In our previous gas analysis study, Co showed much weaker catalytic activity against CH_4 decomposition than Fe metal [47]. We think that this low activity of the Co metal against the CH_4 decomposition leads to the absence of SWCNTs below 50% CH_4 concentrations.

Both Ni and Cu metals showed low catalytic activity. It is consistent that most of works do not use Ni as a catalyst, because of its low catalytic activity toward SWCNT formation

[47]. It is interesting to note that optimized CH_4 concentration observed for Cu metal is high (80%), which contrasts to the Co metal. Because Cu has low carbon solubility and low catalytic activity against CH_4 decomposition, the high CH_4 concentration may be necessary to grow SWCNTs. Also, because H_2 is known to suppress the carbon formation by weak etching effect, low H_2 concentration (i.e., high CH_4 concentration) might be also essential to grow nanotubes over Cu.

Next, thickness dependence of each metal film was studied. We measured the distribution of SWCNT density in a series of patterned metal with respect to the supplied CH_4 concentration (Fig. 4). The colors represent the nanotube density measured by SEM. From Fig. 4a, we can see that the optimal Fe thickness varies with the CH_4 concentration. Under low concentrations (45-55%), thin Fe films gave SWCNTs, while under the high CH_4 concentration (60-85%), thicker Fe films became more catalytically active. This relationship between the CH_4 concentration and the Fe film thickness is related with the size of the metal nanoparticles produced during the heating process, as will be discussed later.

The similar phenomenon, i.e. higher CH_4 concentration extends the upper limits of the metal film thickness for the growth of SWCNTs, was also observed for Ni and Cu metals (Fig. 4c,d). In the case of Ni metal, the SWCNT growth was observed only at very thin region <0.6 nm (Fig. 4c). This can be accounted for by the facile aggregation of Ni nanoparticles at high temperature, thus very thin Ni film can give the nanoparticles whose size is small enough to grow SWCNTs.

3.2. Diameter distributions

The diameters of aligned SWCNTs were studied by resonance Raman spectroscopy with 514.5 nm excitation. A typical Raman spectrum of a SWCNT grown over the Fe catalyst under 70% CH_4 flow is displayed in Fig. 5a. The highest density area, i.e. the yellow region of Fig. 4a, was measured. Clear G-band was observed at ~1595 cm^{-1} which is originated from the graphene network. The D-band appeared at ~1350 cm^{-1} originated from defects or disordered carbon was very weak, indicating that the nanotube is of high quality. Radial breathing mode (RBM) coming from cylindrical nanotube structure was also observed mainly

at 100-200 cm^{-1}. These clear RBM peaks indicate that the aligned tubes are SWCNTs. The nanotube diameter is calculated from the equation, $d=248/\omega$, where ω is the RBM frequency [48].

To estimate the SWCNT diameter distribution, the sample was scanned along several catalyst lines so that the tubes grown from the similar Fe thicknesses are counted. Figure 5b-f compares the diameter distribution measured for different metals and conditions. Although the RBM distribution measured only by single excitation wavelength is not sufficient, it enables qualitative comparison on the relative diameter distribution. The diameter distributions of the aligned SWCNTs formed on plain sapphire surface are generally broad. Because the thermal diffusion and aggregation of metal nanoparticles occurs more easily on the plain sapphire than on nanoporous support materials, the Ostwald ripening is likely to occur to give a wide diameter distribution of metal nanoparticles.

However, when compared with the SWCNTs grown from the Fe 0.7 nm film with 70% CH_4 (Fig. 5b), those grown from the Fe 0.2 nm film with CH_4 45% (Fig. 5c) showed narrower diameter distribution with less large-diameter tubes. Because Fe is catalytically active to nanotube growth, the large-diameter tubes can also be formed under higher CH_4 concentration. As seen from Figs. 5d-5f, the CH_4 concentration influenced the diameter distribution irrespective of the metal catalyst; higher CH_4 concentration tends to give larger diameter tubes.

We measured the AFM images after annealing the Fe patterned substrates under a H_2 gas at 900 ºC for 5 min (without adding CH_4), as shown in Fig. 6. This annealing process produced a number of Fe nanoparticles, and their size and density were correlated with the original metal thickness. We found that a thicker Fe film tends to give larger Fe nanoparticles. It was difficult to observe Fe nanoparticles for very thin Fe films like 0.2 nm. We think that the nanoparticles (or small clusters) formed from the Fe 0.2 nm-thick line are too small to be observed and these particles become larger during flowing CH_4 in the actual CVD process. One can see that thin Fe film (0.4 nm) preferentially gives fine Fe nanoparticles with a diameter smaller than 2 nm (Fig. 6g-i). The relatively large nanoparticles with a diameter of >2 nm occupy only a small fraction, although the reason is

unclear. This size distribution is suitable for the SWCNT growth and well explains the SWCNT distribution observed for thin metal films that suggests the suppression of large-diameter SWCNTs with >2 nm diameter (see Fig. 5c). Because the smaller metal nanoparticles are more facile to be deactivated than the larger ones, the thin metal film catalyzed the nanotube growth at a lower CH_4 concentration (see Fig. 4). However, since the density of nanoparticles is low, the thinner film did not give high density SWCNTs.

When the nominal thickness of a Fe film is 0.7 nm, we obtained the highest SWCNT density under 70% CH_4. As seen in Fig, 6a-c, the 0.7 nm-thick Fe film gave the Fe nanoparticles with a broad diameter distribution which extends to 10 nm diameter. Although the relative ratio of the small Fe nanoparticles suitable for the SWCNT growth (<3 nm) is low, the total nanoparticle density is much higher than that of thinner films. In this case, the high CH_4 concentration is preferable for the high density growth, because relatively large Fe nanoparticles, such as 2 nm diameter, probably catalyze the SWCNT growth efficiently at higher CH_4 concentration.

3.3. Binary metal catalysts

We studied binary metals with gradual film thickness as a catalyst for SWCNT growth. After sputtering the first metal, the mask was rotated by 90º to sputter another metal, as illustrated in Fig. 1a. This gives two-dimensionally distributed metal patterns with gradual film thicknesses. Figure 7 displays the SWCNT density measured for the different combinations of binary metal catalysts under a fixed CH_4 concentration of 70%. Our study revealed that Fe/Co/sapphire and Co/Cu/sapphire gave high SWCNT density. Although Mo is known to promote the SWCNT growth both for Fe and Co metals [43-47], this effect was not observed in our aligned SWCNT arrays. For example, when we used the mixed solution of $Fe(NO_3)_3{\cdot}9H_2O$ nitrate and $MoO_2(acac)_2$ as the catalyst, the enhanced SWCNT density was observed on a-plane sapphire [49]. This result was explained by the increased Fe-Mo metal nanoparticle density on the substrate surface due to nanoparticles stabilization effect of Mo co-catalyst [49]. In the present work, since we use sputtered metal films as a catalyst, the binary metal films may behave differently from the solution of the metal salts: the

heat-induced nanoparticle formation process maybe not be so affected by the addition of Mo metal in the case of the sputtered films.

Binary Fe/Co metal catalysts were further studied by changing the CH_4 concentration. The result is displayed in Fig. 8. At 75-85% CH_4 concentrations, very high SWCNT density of 7~9 tubes/μm was observed. This high density was obtained at the region where the sufficient thicknesses of both Fe and Co metals are deposited. Therefore, this enhanced SWCNT yield is accounted for by a synergetic effect of Fe and Co metals. This synergetic effect of Fe-Co binary metal was also reported for powder catalysts [50-52], but this is the first time demonstrated for the horizontally aligned SWCNTs. Three mechanisms are proposed for the active Fe-Co binary metals supported on porous materials; (i) Fe-Co combination enhances catalytic activity towards CH_4 dissociation [50], (ii) presence of Co prevents the formation of Fe_3C and carbides thereby avoiding deactivation of Fe nanoparticle [51], and (iii) the diffusion of Fe into the surface SiO_2 layer acts as a blocking layer which prevents Co from the diffusion into the SiO_2 and thermal aggregation [52]. In our case, interestingly, the high SWCNT density was seen under wide CH_4 concentration range, and the optimal CH_4 concentration (75-80%) is higher than that on single Fe or Co metal catalyst (70 and 65% for Fe and Co, respectively; see Fig. 3). From this result, we think that this enhanced catalytic activity of Fe-Co binary metal is explained by the mechanism (i), the enhanced dissociation of CH_4 molecules over the Fe-Co alloy nanoparticles.

As shown in Fig. 9, Co/Cu catalyst also showed very high catalytic activity under 70% CH_4 supply. The maximum density of 8~10 tubes/μm was obtained, which is slightly higher than that obtained on the Fe/Co binary catalyst. The improved SWCNT yield using this combination has not been reported as far as we know. Although the density still needs to be improved when compared with the SWCNT density achieved on quartz (~22 tubes/μm [24]), this is the highest density obtained on sapphire. Unlike the Fe/Cu binary catalyst, the Co/Cu catalyst showed high catalytic activity under a limited CH_4 concentration (70%). In addition, the aligned SWCNTs are relatively short, as seen in Fig. 9e. We discussed that Co metal is facile to be deactivated under a high CH_4 concentration (see Fig. 3). On the other hand, Cu metal catalyzes the SWCNT growth under high CH_4 concentration (80%). Therefore, we

infer that the Cu metal contributes to maintain a clean nanoparticle surface by preventing the deposition of excess carbon. As the cleaning effect of Cu is not so high, the SWCNT growth terminates in relatively short time. We note, however, it is likely that Co-Cu forms metal alloy nanoparticles so that a new synergetic effect might contribute the enhanced catalytic activity.

Shown in Fig. 10 is the diameter distributions measured for the high density SWCNT arrays formed on the Fe-Co and Co-Cu binary catalysts. The diameters estimated from the Raman mapping measurements showed a similar distribution with that seen in the corresponding single metal catalysts. More study is necessary for the understanding the enhanced catalytic activity observed in the Fe-Co and Co-Cu combinations for the further improvement of SWCNT density.

4. Conclusions

Catalytic activities of single and binary metal catalysts are systematically studied using a CMD approach with varied CH_4 concentrations. We demonstrate that Fe and Co metal films give high SWCNT density with a density of 4~6 tubes/μm, while Ni and Co give low density of ~1 tube/μm. The CH_4 concentration dependence shows that Fe is reactive in the wide reaction window, while Co is reactive under relatively low CH_4 concentrations. Higher SWCNT densities were obtained for Fe-Co (7~9 tubes/μm) and Co-Cu (8~10 tubes/μm) binary catalysts. The Fe-Co showed high catalytic activity under CH_4 concentrations higher than that used for single Fe or Co metals. The Co-Cu showed high density under a limited CH_4 concentration and the SWCNTs are relatively short. Our work gives new insight into the different catalytic activity of transition metals, and the result will be further developed to grow high density SWCNTs for high performance electronics.

Acknowledgements

We acknowledge the support from the Program for Development of Nanoelectronic Device Technology of NEDO and discussion with Prof. T. Mizutani of Nagoya University. We thank R. Takaki for experimental help.

References

[1] Baughman RH, Zakhidov AA, de Heer WA. Carbon nanotubes–the route toward applications. Science 2002; 297: 787-92.

[2] Javey A, Kim H, Brink M, Wang Q, Ural A, Guo J, et al. High-κ dielectrics for advanced carbon nanotube transistors and logic gates. Nat. Mater. 2002; 1, 241-246.

[3] Yao Z, Kane CL, Dekker C. High-field electrical transport in single-wall carbon nanotubes. Phys. Rev. Lett. 2000; 84: 2941.

[4] S. M. Sze, Physics of Semiconductor Devices, 2nd ed., Wiley-Interscience, 1981, New York.

[5] Izard N, Kazaoui S, Hata K, Okazaki T, Saito T, Iijima S, et al., Semiconductor-enriched single wall carbon nanotube networks applied to field effect transistors. Appl. Phys. Lett. 2008; 92: 243112.

[6] Miyata Y, Yanagi K, Maniwa Y, Kataura H. Highly stabilized conductivity of metallic single wall carbon nanotube thin films. J. Phys. Chem. C 2008; 112: 3591-3596.

[7] Lee CW, Han X, Chen F, Wei J, Chen Y, Park MBC, et al. Solution-processable carbon nanotubes for semiconducting thin-film transistor devices. Adv. Mater. 2010; 22: 1278-1282.

[8] Martel R. Sorting carbon nanotubes for electronics. ACS Nano. 2008; 2: 2195-2199.

[9] Mizuno S, Hata K, Saito T, Ohshima S, Yumura M, Iijima S. Selective matching of catalyst element and carbon source in single-walled carbon nanotube synthesis on silicon substrates. J. Phys. Chem. B 2005; 109: 2632-2637.

[10] Takenobu T, Miura N, Lu SY, Okimoto H, Asano T, Shiraishi M, et al. Ink-jet printing of carbon nanotube thin-film transistors on flexible plastic substrates. Appl. Phys. Exp. 2009; 2: 25005.

[11] Snow ES, Novak JP, Campbell PM, Park D. Random networks of carbon nanotubes as an electronic material. Appl. Phys. Lett. 2003; 82: 2145.

[12] Bradley K, Gabriel JC, Grüner G. Flexible Nanotube Electronics. NanoLett. 2003; 3: 1353-1355.

[13] Shiraishi M, Takenobu T, Iwai T, Iwasa Y, Kataura H, Ata M. Single-walled carbon nanotube aggregates for solution-processed field effect transistors. Chem. Phys. Lett. 2004; 394: 110-113.

[14] Huang, S.; Cai, X.; Liu, J. Growth of Millimeter-long and horizontally aligned single-walled carbon nanotubes on flat substrates. J. Am. Chem. Soc. 2003; 125: 5636-5637.

[15] Yu Z, Li S, Burke P. J. Synthesis of aligned arrays of millimeter long, straight single-walled carbon nanotubes. Chem. Mater. 2004; 16: 3414-3416.

[16] Joselevich E, Lieber C. M. Vectorial growth of metallic and semiconducting single-wall carbon nanotubes. NanoLett. 2002; 2: 1137-1141.

[17] Ural, A.; Li, Y.; Dai, H. Electric-field-aligned growth of single-walled carbon nanotubes on surfaces. Appl. Phys. Lett. 2002, 81, 3464-3466.

[18] Ismach A, Wachtel E, Joselevich E. Atomic-step-remplated formation of single wall carbon nanotube patterns. Ang. Chem. Int. Ed. 2004; 43: 6140-6143.

[19] Ago H, Nakamura K, Ikeda K, Uehara N, Ishigami N, Tsuji M. Aligned growth of isolated single-walled carbon nanotubes programmed by atomic arrangement of substrate surface. Chem. Phys. Lett. 2005; 408: 433-438.

[20] Ago H, Imamoto K, Ishigami N, Ohdo R, Ikeda K, Tsuji M. Competition and cooperation between lattice-oriented growth and step-templated growth of aligned carbon nanotubes on sapphire. Appl. Phys. Lett. 2007; 90: 123112-1-3.

[21] Han S, Liu X, Zhou C. Template-free directional growth of single-walled carbon nanotubes on a- and r-plane sapphire. J. Am. Chem. Soc. 2005; 127: 5294-5295.

[22] Yu Q, Qin G, Li H, Xia Z, Nian Y, Pei S. S. Mechanism of horizontally aligned growth of single-wall carbon nanotubes on r-plane sapphire. J. Phys. Chem. B 2006; 110: 22676-22680.

[23] Kocabas C, Hur S. H, Gaur A, Meitl M. A, Shim M, Rogers J. A. Guided growth of large-scale, horizontally aligned arrays of single-walled carbon nanotubes and their use in thin-film transistors. Small 2005; 1: 1110-1116.

[24] Ding L, Yuan D, Liu J. Growth of high-density parallel arrays of long single-walled carbon nanotubes on quartz substrates. J. Am. Chem. Soc. 2008; 130: 5428-5429.

[25] Phokharatkul D, Ohno Y, Nakano H, Kishimoto S, Mizutani T. High-density horizontally aligned growth of carbon nanotubes with Co nanoparticles deposited by arc-discharge plasma method. Appl. Phys. Lett. 2008; 93: 53112.

[26] Zhang B, Hong G, Peng B, Zhang J, Choi W. M, Kim J. M, Choi J. Y, Liu Z. Grow single-walled carbon nanotubes cross-bar in one batch, J. Phys. Chem. C 2009; 113: 5341-5344.

[27] Rutkowska A, Walker D, Gorfman S, Thomas P. A, Macpherson J. V. Horizontal alignment of chemical vapor-deposited SWNTs on single-crystal quartz surfaces: further evidence for epitaxial alignment. J. Phys. Chem. C 2009, 113, 17087-17096.

[28] Yoshihara N, Ago H, Imamoto K, Tsuji M, Ikuta T, Takahashi K. Horizontally aligned growth of single-walled carbon nanotubes on a surface-modified silicon wafer. J. Phys. Chem. C 2009; 113: 8030-8034.

[29] Orofeo C. M, Ago H, Yoshihara N, Tusji M. Top-down approach to align single-walled carbon nanotubes on silicon substrate. Appl. Phys. Lett. 2009; 94: 53113-1-3.

[30] Kamimura T, Matsumoto K. Controlling Direction of Growth of Carbon Nanotubes on Patterned SiO_2 Substrate. Appl. Phys. Express 2009; 2: 15005.

[31] Ago H, Ishigami N, Yoshihara N, Imamoto K, Akita S, Ikeda K, et al. Visualization of horizontally-aligned single-walled carbon nanotube growth with $^{13}C/^{12}C$ isotopes. J. Phys. Chem. C 2008; 112: 1735-1738.

[32] Kang S. J, Kocabas C, Ozel T, Shim M, Pimparkar N, Alam M. D, et al. High-performance electronics using dense, perfectly aligned arrays of single-walled carbon nanotubes. Nat. Nanotech. 2007; 2: 230-236.

[33] Ishikawa F. N, Chang H. K, Ryu K, Chen P, Badmaev A, De Arco J. G, et al. Transparent electronics based on transfer printed aligned carbon nanotubes on rigid and flexible substrates. ACS Nano 2009; 3: 73-79.

[34] Guo J, Hasan S, Javey A, Bosman G, Lundstron M. IEEE Trans. Nanotech. 2005; 4: 715-721.

[35] Kocabas C, Kang S. J, Ozel T, Shim M, Rogers J. A. Improved synthesis of aligned arrays of single-walled carbon nanotubes and their implementation in thin film type

transistors. J. Phys. Chem. C 2007, 111, 17879-17886.

[36] Akinwande D, Patil N, Lin A, Nishi Y, Wong H.-S. P. Surface science of catalyst dynamics for aligned carbon nanotube synthesis on a full-scale quartz wafer. J. Phys. Chem. C 2009; 113: 8002-8008.

[37] Li B, Cao X, Huang X, Lu G, Huang Y, Goh C. F, et al. Facile ‘‘needle-scratching’’ method for fast catalyst patterns used for large-scale growth of densely aligned single-walled carbon-nanotube arrays. Small 2009; 5: 2061-2065.

[38] Ding L, Yuan D, Liu J. Growth of high-density parallel arrays of long single-walled carbon nanotubes on quartz substrates. J. Am. Chem. Soc. 2008; 130: 5428-5429.

[39] Ishigami N, Ago H, Nishi T, Ikeda K, Tsuji M, Ikuta T, et al. Unidirectional growth of single-walled carbon nanotubes. J. Am. Chem. Soc. 2008; 130: 17264-17265

[40] Ago H, Nishi T, Imamoto K, Ishigami N, Tsuji M, Ikuta et al. Orthogonal growth of horizontally-aligned single-walled carbon nanotube arrays. J. Phys. Chem. C, 2010; 114:.12925-12930.

[41] Ago H, Imamoto K, Nishi T, Tsuji M, Ikuta T, Takahashi K, et al. Direct growth of bent carbon nanotubes on surface engineered sapphire. J. Phys. Chem. C 2009; 113: 13121-13124.

[42] Ishigami N, Ago H, Imamoto K, Tsuji M, Iakoubovskii K, Minami N. Crystal plane dependent growth of aligned single-walled carbon nanotubes on sapphire. J. Am. Chem. Soc. 2008; 130: 9918-9924.

[43] Murakami Y, Chiashi S, Miyauchi Y, Hu M, Ogura M, Okubo T, et al. Growth of vertically aligned single-walled carbon nanotube films on quartz substrates and their optical anisotropy. Chem. Phys. Lett. 2004; 385: 298-303.

[44] Noda S, Sugime H, Osawa T, Tsuji Y, Chiashi S, Murakami Y, et al. A simple combinatorial method to discover Co–Mo binary catalysts that grow vertically aligned single-walled carbon nanotubes. Carbon; 2006; 44: 1414-1419.

[45] Bachilo SM, Balzano L, Herrera JE, Pompeo F, Resasco DE, Weisman RB. Narrow (*n*,*m*)-distribution of single-walled carbon nanotubes grown using a sSolid supported catalyst. J. Am. Chem. Soc. 2003; 125: 11186-11187.

[46] Cassell AM, Raymakers JA, Kong J, Dai H. Large scale CVD synthesis of single-walled

carbon nanotubes. J. Phys. Chem. B 1999; 103: 6484-6492

[47] Ago H, Uehara N, Yoshihara N, Tsuji M, Yumura M, Tomonaga N, et al. Gas analysis of the CVD process for high yield growth of carbon nanotubes over metal-supported catalysts. Carbon 2006; 44: 2912-2918.

[48] Jorio A, Saito R, Hafner JH, Lieber CM, Hunter M, McClure T, et al. Structural (*n*,*m*) determination of isolated single-wall carbon nanotubes by resonant Raman scattering. Phys. Rev. Lett. 2001; 86: 1118-1121.

[49] Ago H, Uehara N, Ikeda K, Ohdo R, Nakamura K, Tsuji M. Synthesis of horizontally-aligned single-walled carbon nanotubes with controllable density on sapphire surface and polarized Raman spectroscopy. Chem. Phys. Lett. 2006; 421: 399-403.

[50] Xu Y, Li Z, Dervishi E, Saini V, Cui J, Biris AR, Lupu D, Biris AS. Surface area and thermal stability effect of the MgO supported catalysts for the synthesis of carbon nanotubes. J. Mater. Chem. 2008; 18: 5738-5745.

[51] Flahaut E, Govindaraj A, Peigney A, Laurent Ch, Rousset A, Rao CNR. Synthesis of single-walled carbon nanotubes using binary (Fe, Co, Ni) alloy nanoparticles prepared in situ by the reduction of oxide solid solutions. Chem. Phys. Lett. 1999; 300: 236-242.

[52] Murakami T, Mitikami K, Ishigaki S, Matsumoto K, Nishio K, Isshiki T, et al. Catalytic mechanism of a Fe-Co bimetallic system for efficient growth of single-walled carbon nanotubes on Si/SiO_2 substrates. J. Appl. Phys. 2006; 100: 94303.

Figure captions

Figure 1. (a) Schematic of the preparation method of the stripe-pattern of metal films with gradual film thicknesses. This schematic shows the deposition of a double-layer film for binary metal catalyst. Photoresist which is used to pattern the metal film is omitted for simplicity. (b) Detailed structure of the slit mask and a sapphire substrate patterned with photoresist. (c) Nominal thicknesses of metal films sputtered on r-plane sapphire. Lines are fitted exponential curves. (d) Image of horizontally aligned SWCNTs grown from the patterned catalysts.

Figure 2. SEM images of SWCNTs grown from the patterned catalysts: (a) Fe, (b) Co, (c) Ni, and (d) Cu. The nominal metal thickness and CH_4 concentration are 0.7 nm-70%, 0.8 nm-65%, 0.5 nm-75%, and 1.0 nm-80% for Fe, Co, Ni, and Cu, respectively.

Figure 3. Comparison of SWCNT density plotted as a function of CH_4 concentration during the CVD growth. Total flow rates are fixed to be 350 ccm. The highest density observed on each substrate is extracted regardless of the metal thickness. The SWCNT density was counted by SEM.

Figure 4. The spatial distribution of SWCNT density on a patterned substrate: (a) Fe, (b) Co, (c) Ni, and (d) Cu. The SWCNT densities were measured for different CH_4 concentrations. The origin is set 3 mm apart from the center of the slit, as illustrated in Fig. 1b.

Figure 5. (a) Raman spectrum of a SWCNT grown from the Fe catalyst under 70% CH_4. The spectrum of highest density area, yellow region shown in Fig. 4a, is measured. The excitation wavelength and spot size are 514.5 nm and ~1 μm, respectively. (b-f) Diameter distributions of SWCNTs observed on different metal catalysts and under different CH_4 concentrations. The nanotube diameter is estimated from the RBM freauency of the Raman spectrum measured using 514.5 nm excitation wavelength.

Figure 6. AFM images (a,b,d,e,g,h) and diameter distributions (c,f,i) of the Fe nanoparticles observed after annealing with H_2 at 900 ºC for 5 min. Nominal thicknesses of the initial Fe films are (a-c) 0.7 nm, (d-f) 0.6-0.5 nm, and (g-i) 0.4 nm. The nanoparticle diameter is determined from the corresponding AFM height, and the total numbers of counted Fe nanoparticles are 100 for all the histograms.

Figure 7. Contour plots SWCNT densities synthesized on the binary metal catalysts with different metal combinations. The thicknesses of metal films are nominal value estimated from the fitting curves shown in Fig. 1. The CH_4 concentration used for CVD is 70%.

Figure 8. (a-e) Contour plots SWCNT densities observed for the patterned Fe/Co/sapphire substrates with different CH_4 concentrations. (f) SEM image of aligned SWNTs grown under 75% CH_4 concentration.

Figure 9. (a-d) Contour plots SWCNT densities observed for the patterned Co/Cu/sapphire substrates with different CH_4 concentrations. (e,f) SEM images of aligned SWNTs grown under 70% CH_4 concentration.

Figure 10. Diameter distributions of carbon nanotubes obtained for the Fe/Co (a) and Co/Cu (b) catalysts. The highest density area was measured for each catalyst. The diameters are measured by the same method used in Fig. 5.

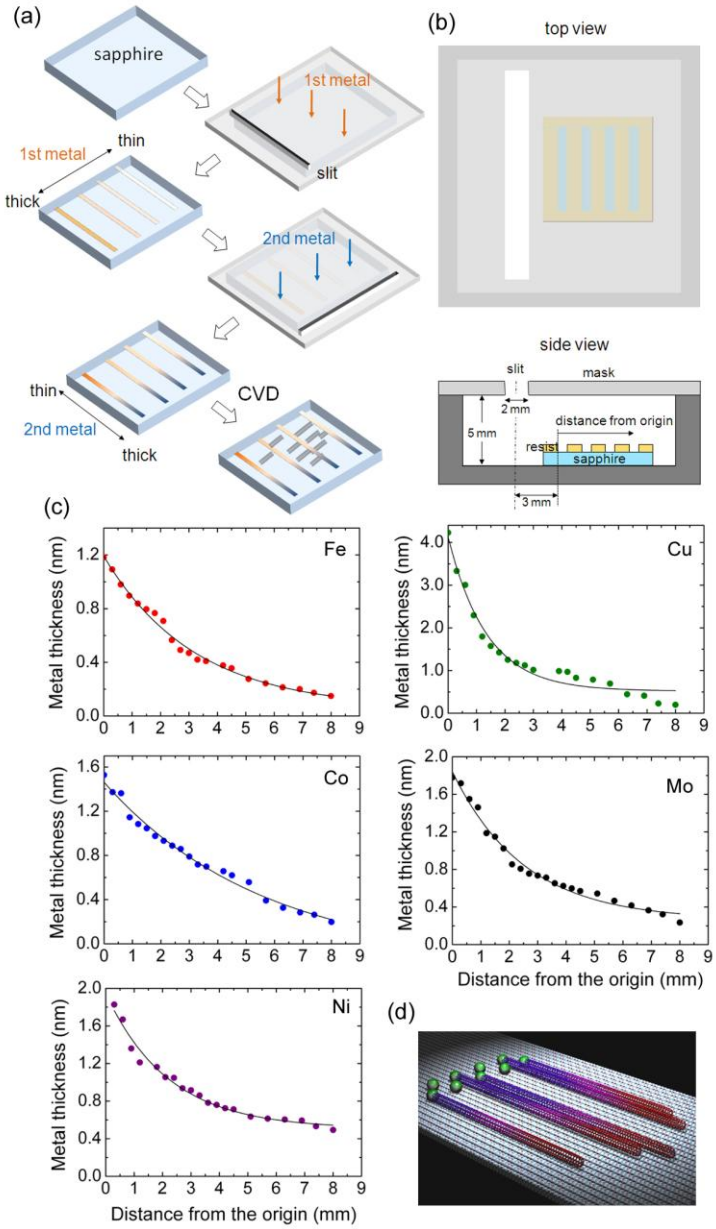

Figure 1. H. Ago *et al.*

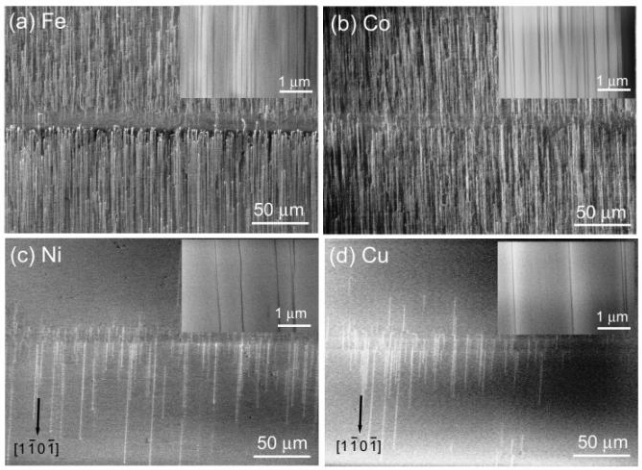

Figure 2. H. Ago *et al.*

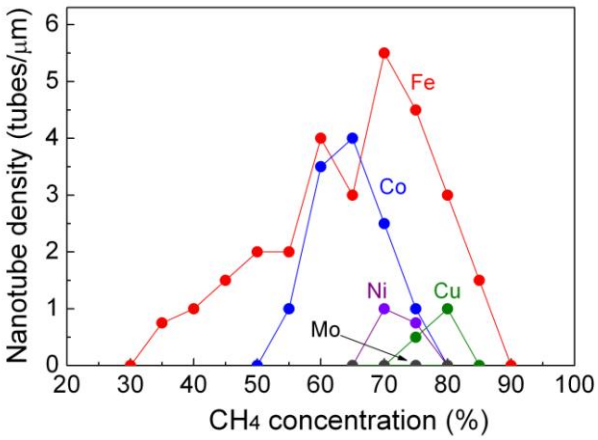

Figure 3. H. Ago *et al.*

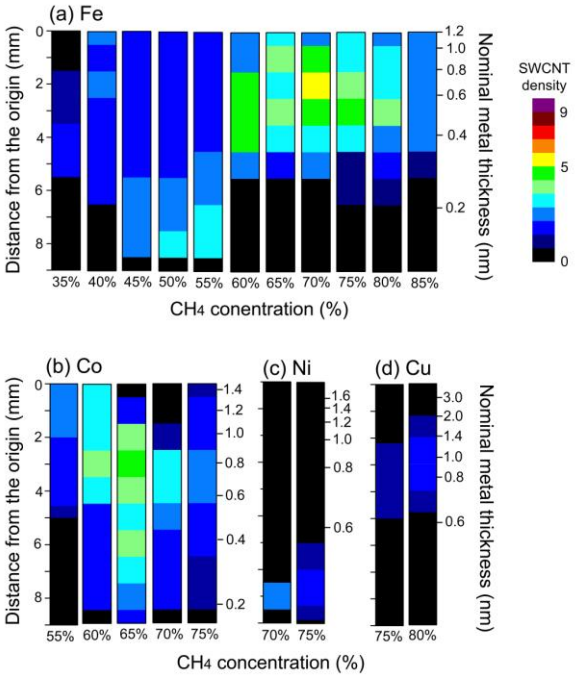

Figure 4. H. Ago *et al.*

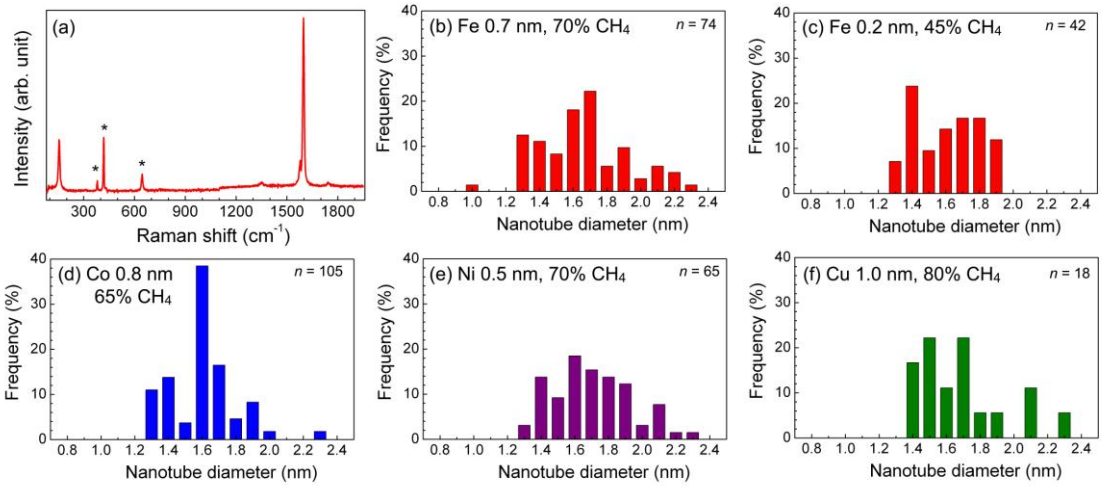

Figure 5. H. Ago *et al.*

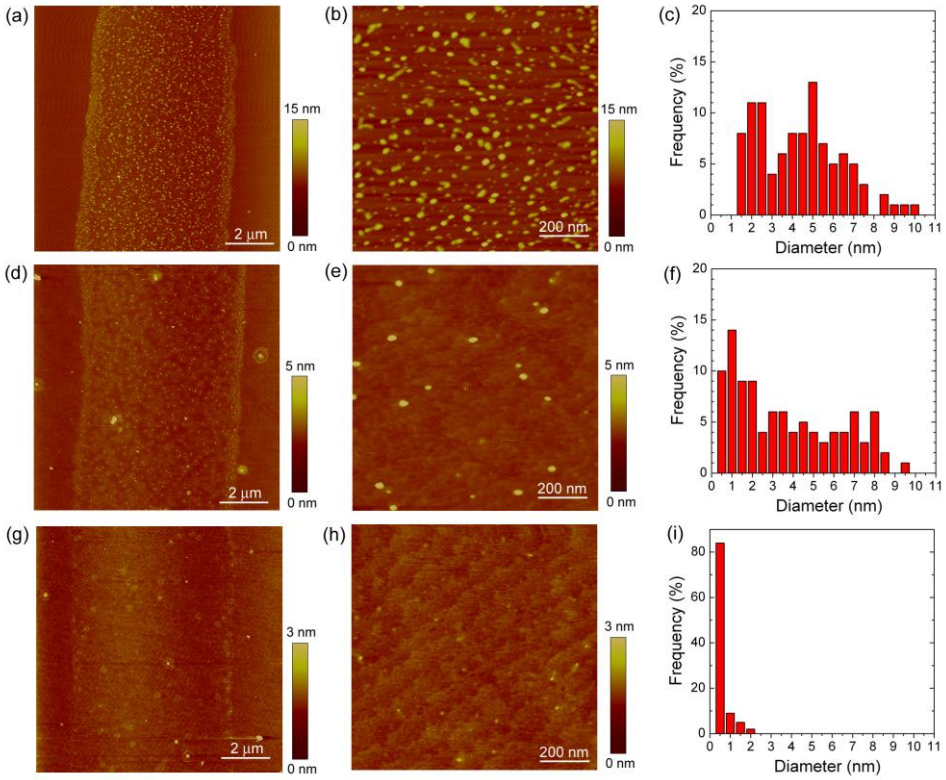

Figure 6. H. Ago *et al*

.

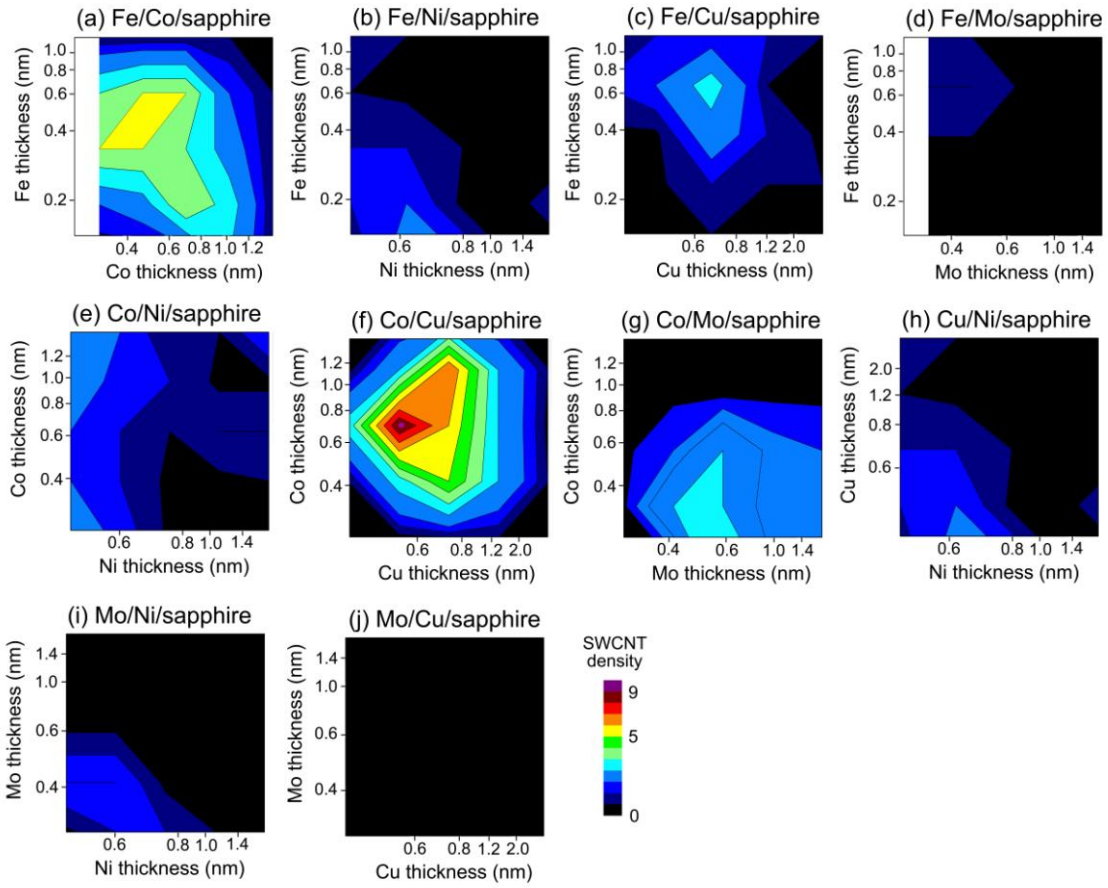

Figure 7. H. Ago *et al*

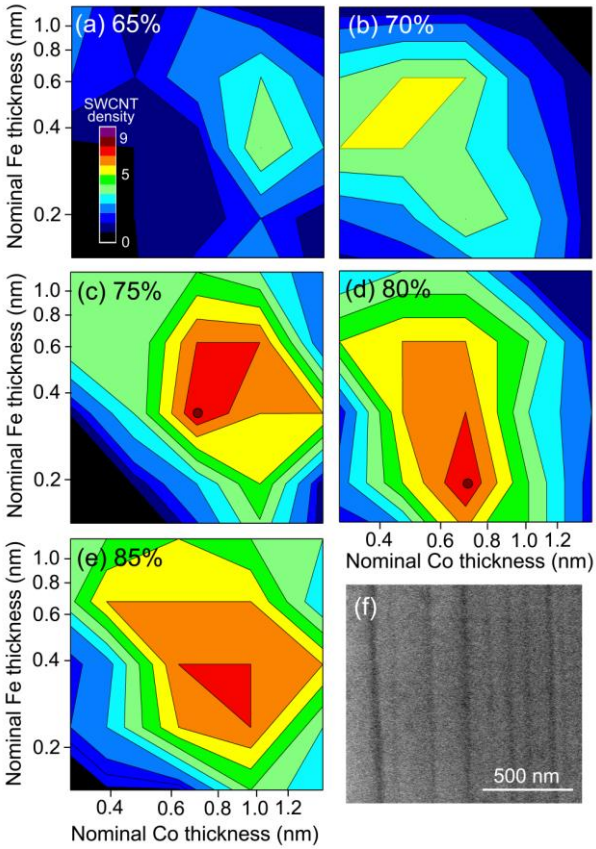

Figure 8. H. Ago *et al.*

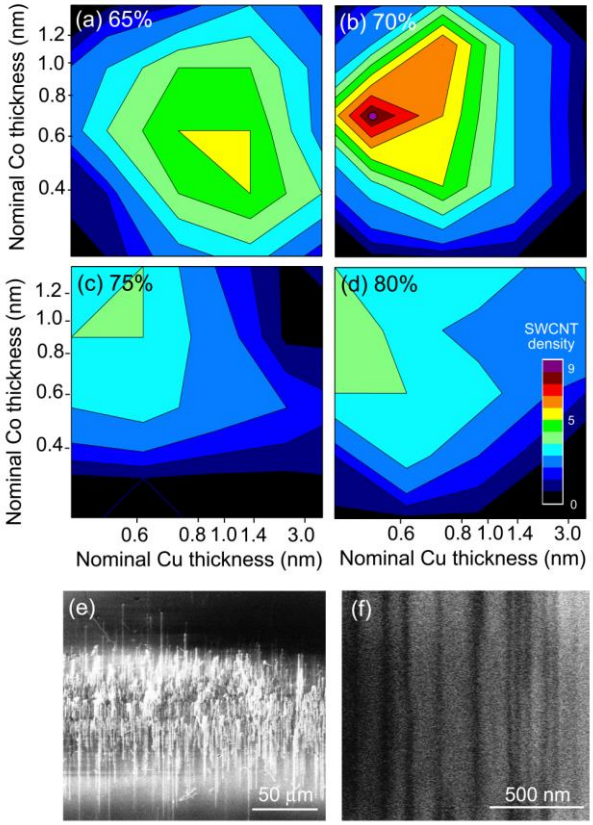

Figure 9. H. Ago *et al.*

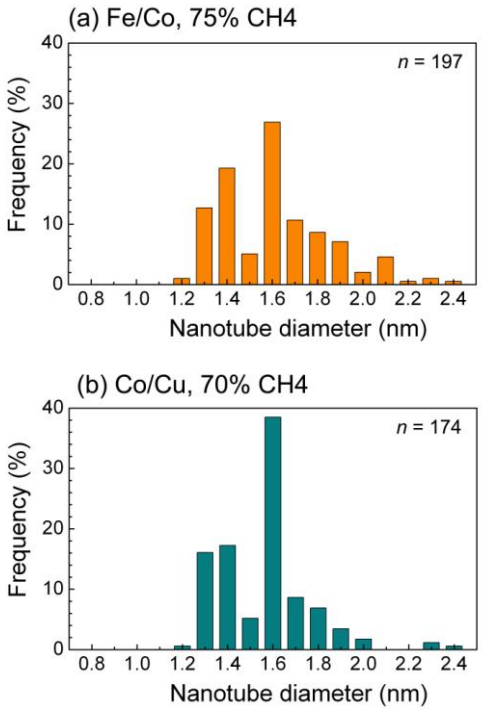

Figure 10. H. Ago *et al.*